COMMUNICATION

Check for updates

Channel current analysis estimates the pore-formation and the penetration of transmembrane peptides†

Yusuke Sekiya,[a] Shungo Sakashita,[b] Keisuke Shimizu,[a] Kenji Usui [ID][b] and Ryuji Kawano [ID] *[a]

We measured the current signal of the transmembrane model peptides using the barrel-stave, toroidal pore, and penetration models in order to establish a precise assignment of the channel signals. In addition, we analyzed the spike signals to estimate the membrane penetration of model cell-penetration peptides of different lengths.

Short transmembrane peptides (∼50 amino acids) including pore-forming or cell-penetration peptides (CPPs) have important biological functions such as antimicrobial activities or mass transport through cell membranes.[1,2] Elucidating the structure–function associations of transmembrane peptides is of considerable scientific interest for the understanding of mechanisms and for medical applications; however, the development of methodologies for structural analysis in lipid membranes remains a challenge. In the case of large membrane proteins such as ion channels or receptors (∼100 kDa), protein structures have been experimentally elucidated with high accuracy using X-ray crystallography, electron microscopy, and atomic force microscopy.[3–5] However, in the case of short peptides, the determination of the structure is impossible using the above methods because of their small molecular size. While spectroscopic methods such as solid-state NMR,[6,7] circular dichroism (CD) spectroscopy, including oriented CD with liposomes,[8,9] and surface plasmon resonance (SPR)[10,11] are conventionally used for this analysis, high accuracy of the structure is difficult to obtain using spectroscopic methods.

We proposed that a channel current method would be an effective tool for the structural analysis of pore-forming peptides such as antimicrobial peptides (AMPs).[12–14] AMPs kill bacteria by forming pores or defects in their cell membranes, resulting in cell lysis. Pore formation can be monitored *via*

channel-current measurement using a planar bilayer lipid membrane (pBLM) as the artificial cell membrane; current signals associated with various types of transmembrane peptide structures are shown in Fig. 1a–c. Traditionally, channel current measurements using pBLMs require considerable operator proficiency for membrane formation, and the stability of these membranes is not enough to acquire large datasets for stochastic analysis. We have developed a stable and reproducible method for pBLM formation using microfabricated and microfluidic technologies;[15,16] the microdevice is presented in Fig. 1d. Our proposed droplet contact method uses two microdroplets surrounding a lipid monolayer, and it brings these droplets into contact with each other forming a lipid bilayer at the interface of the droplets. Due to the high stability of the pBLM in this method, we have successfully measured several ion channels,[16] pore-forming proteins,[12] and synthetic channels,[17] obtaining large datasets, and we have also applied parallel nanopore measurements for single molecule detection.[18–20]

Several different current–signal shapes appeared in the channel recordings, and we classified the four types of current signals according to the signal classification of synthetic channels, as previously proposed.[21] Furthermore, we have attempted to assign these signals to the specific models of previously reported peptide structures,[1,22] as described below.[14]

(1) *Step-like signal*: In this type of current signal, the current jumps up orthogonally and maintains a plateau state. This signal can apply to the "barrel-stave model", wherein transmembrane peptides are tightly assembled with each other and form a rigid circular pore (Fig. 1a).

(2) *Multi-level signal*: In this type of current signal, the current shows fluctuation after jumping up and returns to the initial state. This current may indicate a "toroidal" model, wherein transmembrane peptides form a pore with lipids. In this model, the size of the pore can change dynamically with or without the participation of the lipid between the monomers (Fig. 1b).

(3) *Erratic signal*: In this type of current signal, the current presents random increases with fluctuation. We assigned this

[a]Department of Biotechnology and Life Science, Tokyo University of Agriculture and Technology, 2-24-16 Naka-cho, Koganei, Tokyo 184-8588, Japan.
E-mail: rjkawano@cc.tuat.ac.jp
[b]FIRST (Faculty of Frontiers of Innovative Research in Science and Technology),
Konan University, 7-1-20 Minatojima-minamimachi, Chuo-ku, Kobe 650-0047, Japan.
†Electronic supplementary information (ESI) available: All experimental procedures and figures. See DOI: 10.1039/c8an00243f
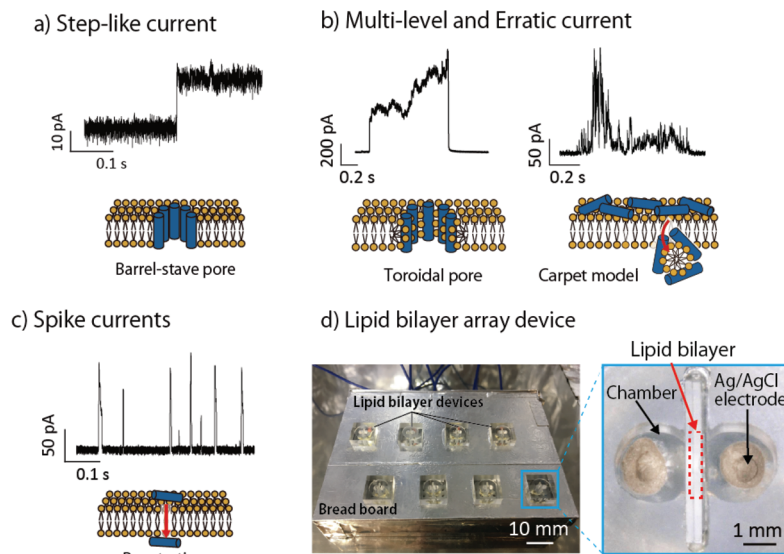
a) Step-like current

b) Multi-level and Erratic current

Barrel-stave pore

Toroidal pore

Carpet model

c) Spike currents

Penetration

d) Lipid bilayer array device

Lipid bilayer devices

Bread board

10 mm

Lipid bilayer

Chamber

Ag/AgCl electrode

1 mm

Fig. 1 Classification of the channel current signals of pore-forming peptides and possible models of the mechanisms from among those previously proposed. The typical current signals of step-like (a), multi-level and erratic (b), and spike (c) with an illustration of our proposed models. (d) Photograph of the pBLM array. In this system, eight detachable devices prepare the eight independent lipid bilayers simultaneously. A device has two chambers with electrodes that are separated by a separator.

signal to the "carpet" model. The carpet model has been described as peptides that bind parallel to the lipid bilayer surface and, after reaching sufficient coverage, unwrap lipids as a peptide–lipid cluster from the membrane, similar to a detergent. The random current behavior of the erratic signal might be caused by the random size of the cluster (Fig. 1b).

(4) *Spike signal*: In this type of current signal, the current suddenly increases and then returns to the baseline over a period of less than 20 ms. This signal indicates an instantaneous membrane defect. We applied this signal to peptide permeation through the membrane (Fig. 1c).

Detailed signal classification is described in the ESI.†

To construct a more probable assignment, in this study, we measured three characteristic peptides (Table S1†): magainin-1 was used as the toroidal pore model peptide,[23,24] alamethicin was used as the barrel-stave dominant peptide,[25,26] and the LK peptide was used as the CPP.[27,28] The current signals of these peptides were classified using the above-mentioned classification.

Magainin-1 is a popular AMP, discovered in the skin of the African clawed frog *Xenopus laevis*.[24] In the current recordings, all 4 current signals were observed, as shown in Fig. 2a. These peptides should interact not only with each other but also with lipid molecules. They sometimes self-assemble into a barrel-stave pore, showing step-like signals. In other cases, they form the toroidal pore with lipid molecules or a carpet model structure. They also directly penetrate through the lipid membrane. The signal classification in Fig. 2a suggests that all the 4 models randomly appeared in the magainin-1 measurements.

Fig. 2b represents the results of alamethicin measurements. Alamethicin is a 20-residue sequence high in 2-aminoisobuty-
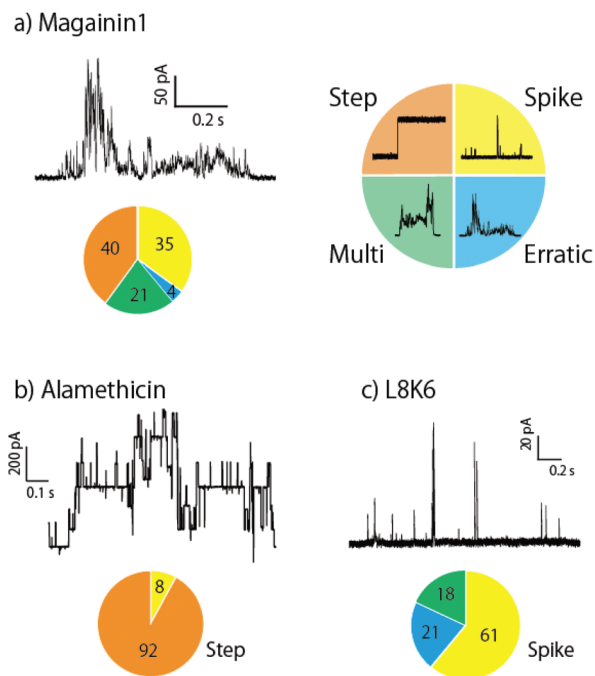

a) Magainin1

Step

Spike

Multi

Erratic

b) Alamethicin

Step

c) L8K6

Spike

Fig. 2 Signal classification of three kinds of peptides. The number of circular graphs indicates the percentages of each signal ($n = 87$–146).

ric acid (Aib) that forms a 3_{10}-helical (3 residues per turn) structure.[29] This peptide is well known for its formation of the barrel-stave pore. In fact, the obtained currents showed the step-like signal in over 90% of all the observed signals. The barrel-stave structure forms a rigid transmembrane pore because of the strong peptide–peptide interactions. The

current fluctuating up and down reflects the additional monomer insertion into the assembling pore, or the desorption of monomers from the pore.[30]

LK peptides consist of a leucine (L)–lysine (K) sequence, and they are well known as CPPs.[28,31] The single LK peptide unit is [LKKLLKL], named L4K3. In this study, we used several lengths of LK peptides: L8K6, L12K9, and L16K12 named [LKKLLKL]₂, [LKKLLKL]₃, and [LKKLLKL]₄, respectively. The LK peptides have an α-helical structure and have periodic distribution of hydrophobic and hydrophilic regions in the peptide, which serve to stabilize the peptide's secondary structure.[32] Although arginine-rich peptides (*e.g.*, R9) are also well known as CPPs,[33] their secondary structure is almost a random coil. Therefore, we selected α-helical LK peptides as the membrane penetration peptides to maintain a consistent secondary structure across all the selected experimental peptides. Fig. 2c depicts the typical current traces and the signal classification of the L8K6 peptide. The spike signal was dominant in this measurement, suggesting that the peptides may form lipid membrane defects momentarily as they translocate through the membrane, as proposed by the Shai–Matsuzaki–Huang model.[34] Although most conventional methods require fluorescent labeling to study membrane penetration, the current recording method does not require fluorescent labeling; therefore, this direct observation of the penetration phenomenon reveals the molecular mechanism of CPP directly.

Next, we attempted to analyze the spike signals of the L8K6 peptide using 3 parameters: the current amplitude, which gives information on the size of the defect in the membrane; the duration time, which reflects the duration of the defect formation; and the time between spike signals, which shows the event frequency of the penetration (Fig. 3a). Fig. 3b depicts the

scatter plots for the current amplitudes and duration time of the L8K6 peptide. The amplitude and duration range from 10 to 100 pA and from 0.1 to 10 ms, respectively. The dependence of these 3 parameters on peptide length was also studied. The duration and peak amplitude did not reveal significant differences between different peptide lengths, although the values of L12K9 were slightly lower than those of all other peptides (Fig. 3c and d). However, the time between peaks was the highest for L12K9, as shown in Fig. 3e. The histograms and values of all data are presented in Fig. S2† and Table 1. The peak in Fig. 3e indicates that the kinetics of membrane penetration decreases with increasing molecular size up to L12K9 whereas penetration dynamics are similar regardless of size. However, regarding the kinetics of L16K12, the event frequency increased even in the largest molecular structure. This peptide forms a strong α-helical structure in the aqueous phase, as observed from circular dichroism measurements (Fig. S3b†), which may induce peptide binding on the membrane surface. These peptides show relatively higher event frequency, which might be owing to their concentration at the membrane surface. In addition, the length of L16K12 (*ca.* 4 nm: the length of the [LKKLLKL] unit is *ca.* 1 nm) is almost compar-

Table 1 Properties of LK peptides. Helicity was calculated using [θ] 222 nm. Rate constant [s⁻¹] is the reciprocal of time between spikes [s]. Duration time, peak current, and rate constant are median values (*n* > 100)

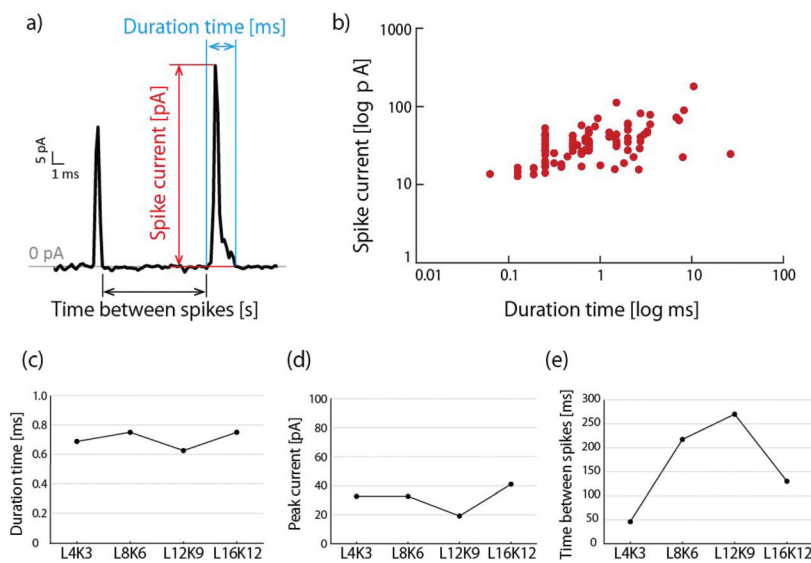|	L4K3	L8K6	L12K9	L16K12
Helicity, buffer [%]	0	0	1.3	58.7
Helicity, liposome [%]	0	15.5	55.8	58.5
Duration time [ms]	0.69	0.75	0.63	0.75
Peak current [pA]	32.7	32.7	19.1	41.0
Rate constant [s⁻¹]	21.7	4.08	3.71	7.68

Fig. 3 (a) Typical current–time spike signal traces of the L8K6 peptide. We analysed the spike current amplitude (red), duration time (blue), and time between spikes (black). (b) Scatter plots of peak current amplitudes and duration time of L8K6 peptides. The repeat length dependency of the LK peptides for (c) the duration time, (d) the peak current, and (e) time between spikes, as mean values. Histograms of all data are shown in Fig. S2.†

able to the thickness of the lipid bilayer in this system. This might cause the higher event frequency. The event rate constant of each peptide is summarized in Table 1. These values are much higher than the value of tat peptide uptake in living cells ($\sim 10^{-3}$ s^{-1}),[2] implying higher membrane penetration kinetics in this system.

In summary, to reveal the molecular mechanism of membrane penetration by short peptides in the lipid bilayer, we classified the current signals of three α-helical peptides using the microfabricated pBLM device, and assigned the signals to the possible structural models in a lipid membrane. The step, multi-level/erratic, and spike signals are assigned as barrel-stave, toroidal pore, and penetration models, respectively, using three typical model peptides: magainin-1, alamethicin, and LK peptides. In addition, we analyzed the spike signals assigned to the membrane penetration, and concluded that the dynamics and kinetics of the membrane penetration may be estimated using the spike amplitude, duration time, and rate constant. Our proposed method using channel current analysis could be a strong candidate for investigating membrane binding peptides at the molecular level.

Conflicts of interest

There are no conflicts to declare.

Acknowledgements

Notes and references

1 K. A. Brogden, *Nat. Rev. Microbiol.*, 2005, **3**, 238–250.
2 M. Zorko and U. Langel, *Adv. Drug Delivery Rev.*, 2005, **57**, 529–545.
3 B. Hille, *Ion channels of excitable membranes*, Sinauer, Sunderland, Mass., 3rd edn, 2001.
4 E. Gouaux and R. MacKinnon, *Science*, 2005, **310**, 1461–1465.
5 D. M. Rosenbaum, S. G. F. Rasmussen and B. K. Kobilka, *Nature*, 2009, **459**, 356–363.
6 B. Bechinger, *Biochim. Biophys. Acta, Biomembr.*, 1999, **1462**, 157–183.
7 A. Naito and I. Kawamura, *Biochim. Biophys. Acta, Biomembr.*, 2007, **1768**, 1900–1912.
8 L. Yang, T. A. Harroun, T. M. Weiss, L. Ding and H. W. Huang, *Biophys. J.*, 2001, **81**, 1475–1485.
9 H. W. Huang, *Biochim. Biophys. Acta, Biomembr.*, 2006, **1758**, 1292–1302.
10 N. Papo and Y. Shai, *Peptides*, 2003, **24**, 1693–1703.
11 M. L. Mangoni, N. Papo, J. M. Saugar, D. Barra, Y. C. Shai, M. Simmaco and L. Rivas, *Biochemistry*, 2006, **45**, 4266–4276.
12 H. Watanabe, A. Gubbiotti, M. Chinappi, N. Takai, K. Tanaka, K. Tsumoto and R. Kawano, *Anal. Chem.*, 2017, **89**, 11269–11277.
13 T. Kunthic, H. Watanabe, R. Kawano, Y. Tanaka, B. Promdonkoy, M. Yao and P. Boonserm, *Biochim. Biophys. Acta, Biomembr.*, 2017, 2234–2241.
14 H. Watanabe and R. Kawano, *Anal. Sci.*, 2016, **32**, 57–60.
15 M. Ohara, Y. Sekiya and R. Kawano, *Electrochemistry*, 2016, **84**, 338–341.
16 R. Kawano, Y. Tsuji, K. Sato, T. Osaki, K. Kamiya, M. Hirano, T. Ide, N. Miki and S. Takeuchi, *Sci. Rep.*, 2013, **3**, 1995.
17 R. Kawano, N. Horike, Y. Hijikata, M. Kondo, A. Carne-Sanchez, P. Larpent, S. Ikemura, T. Osaki, K. Kamiya, S. Kitagawa, S. Takeuchi and S. Furukawa, *Chem*, 2017, **2**, 393–403.
18 H. L. Zhang, M. Hiratani, K. Nagaoka and R. Kawano, *Nanoscale*, 2017, **9**, 16124–16127.
19 M. Ohara, M. Takinoue and R. Kawano, *ACS Synth. Biol.*, 2017, **6**, 1427–1432.
20 M. Hiratani, M. Ohara and R. Kawano, *Anal. Chem.*, 2017, **89**, 2312–2317.
21 J. K. W. Chui and T. M. Fyles, *Chem. Soc. Rev.*, 2012, **41**, 148–175.
22 M. N. Melo, R. Ferre and M. Castanho, *Nat. Rev. Microbiol.*, 2009, **7**, 245–250.
23 K. Matsuzaki, *Biochim. Biophys. Acta, Biomembr.*, 1999, **1462**, 1–10.
24 S. J. Ludtke, K. He, W. T. Heller, T. A. Harroun, L. Yang and H. W. Huang, *Biochem.*, 1996, **35**, 13723–13728.
25 G. A. Woolley and B. A. Wallace, *J. Membr. Biol.*, 1992, **129**, 109–136.
26 D. P. Tieleman, B. Hess and M. S. P. Sansom, *Biophys. J.*, 2002, **83**, 2393–2407.
27 J. A. Cox, M. Comte, J. E. Fitton and W. F. Degrado, *J. Biol. Chem.*, 1985, **260**, 2527–2534.
28 S. Jang, S. Hyun, S. Kim, S. Lee, I. S. Lee, M. Baba, Y. Lee and J. Yu, *Angew. Chem., – Int. Ed.*, 2014, **53**, 10086–10089.
29 B. Leitgeb, A. Szekeres, L. Manczinger, C. Vagvolgyi and L. Kredics, *Chem. Biodiversity*, 2007, **4**, 1027–1051.
30 G. A. Woolley, *Chem. Biodiversity*, 2007, **4**, 1323–1337.
31 K. Usui, T. Kikuchi, M. Mie, E. Kobatake and H. Mihara, *Bioorg. Med. Chem.*, 2013, **21**, 2560–2567.
32 S. Kim, S. Hyun, Y. Lee and J. Yu, *Biomacromolecules*, 2016, **17**, 3007–3015.
33 S. Futaki, T. Suzuki, W. Ohashi, T. Yagami, S. Tanaka, K. Ueda and Y. Sugiura, *J. Biol. Chem.*, 2001, **276**, 5836–5840.
34 M. Zasloff, *Nature*, 2002, **415**, 389–395.